Mon. Not. R. Astron. Soc. **000**, 1–16 (1999) Printed 21 June 2007 (MN LATEX style file v1.4)

Circumnuclear regions in barred spiral galaxies I. Near-infrared imaging⋆

D. Pérez–Ramírez[1], J. H. Knapen[1,2†], R. F. Peletier[3,4], S. Laine[1,5], R. Doyon[6†] and D. Nadeau[6†]

[1] *Department of Physical Sciences, University of Hertfordshire, Hatfield, Herts AL10 9AB, UK. E-mail dperez,knapen@star.herts.ac.uk*
[2] *On leave at Isaac Newton Group of Telescopes, Apartado 321, Santa Cruz de La Palma, E-38700 Spain*
[3] *Department of Physics, University of Durham, South Road, Durham, DH1 3LE, UK*
[4] *School of Physics and Astronomy, University of Nottingham, University Park, Nottingham NG7 2RD , UK (present address)*
[5] *Department of Physics & Astronomy, University of Kentucky, Lexington, KY 40506-0055, USA (present address)*
[6] *Observatoire du Mont Mégantic and Département de Physique, Université de Montréal, C.P. 6128, Succursale Centre Ville, Montréal (Québec), H3C 3J7 Canada, E-mail nadeau,doyon@astro.umontreal.ca*

Accepted 24 February 2000; Received; in original form

ABSTRACT

We present sub-arcsecond resolution ground-based near-infrared images of the central regions of a sample of twelve barred galaxies with circumnuclear star formation activity, which is organized in ring-like regions typically one kiloparsec in diameter. We also present *Hubble Space Telescope* near-infrared images of ten of our sample galaxies, and compare them with our ground-based data. Although our sample galaxies were selected for the presence of circumnuclear star formation activity, our broad-band near-infrared images are heterogeneous, showing a substantial amount of small-scale structure in some galaxies, and practically none in others. We argue that, where it exists, this structure is caused by young stars, which also cause the characteristic bumps or changes in slope in the radial profiles of ellipticity, major axis position angle, surface brightness and colour at the radius of the circumnuclear ring in most of our sample galaxies. In 7 out of 10 *HST* images, star formation in the nuclear ring is clearly visible as a large number of small emitting regions, organised into spiral arm fragments, which are accompanied by dust lanes. NIR colour index maps show much more clearly the location of dust lanes and, in certain cases, regions of star formation than single broad-band images. Circumnuclear spiral structure thus outlined appears to be common in barred spiral galaxies with circumnuclear star formation.

Key words: galaxies: spiral – galaxies: starburst – galaxies: evolution – galaxies: structure – infrared: galaxies

1 INTRODUCTION

Observations and modelling of the circumnuclear regions (CNRs) of barred galaxies give important clues about the nature of active galactic nuclei (AGN), (circum)nuclear starbursts and the gas dynamics in the central kpc (e.g. Knapen et al. 1995a,b; Buta & Combes 1996; Elmegreen et al. 1997; Quillen et al. 1999; Regan & Mulchaey 1999; see also reviews by Knapen 1999 and Shlosman 1999).

The presence of non-axisymmetries, such as oval distortions or bars, in the gravitational potential of a disc galaxy can lead to the infall of gaseous material, from galactocentric radii of a few kpc, into the central kpc. The nonaxisymmetry facilitates the removal of angular momentum from the gas, and directs it into the CNR or possibly the nucleus (Shlosman et al. 1990; Athanassoula 1992; Phinney 1994). This gas fuelling process is expected to induce morphological signatures in the bars and CNRs, which are useful tools in the understanding of the dynamics and kinematics of galax-

⋆ Partly based on observations made with the NASA/ESA *Hubble Space Telescope*, obtained from the data archive at the Space Telescope Science Institute, which is operated by the Association of Universities for Research in Astronomy, Inc. under NASA contract NAS 5-26555.

† Visiting Astronomer, Canada–France–Hawaii Telescope operated by the National Research Council of Canada, the Centre National de la Recherche Scientifique de France and the University of Hawaii.

Object	Type	Velocity km s^{-1}	Distance Mpc	Scale pc/arcsec	CNR Features	Nuclear activity	Date of observation	Passbands
NGC 1300	(R')SB(s)bc	1568	20.9	101	Ring	—	05/11/95	JHK
NGC 1530	SB(rs)b	2461	32.8	159	Ring+spiral	—	05/11/95	JHK
NGC 2903	SAB(rs)bc	556	7.4	36	Ring	Starburst	05/11/95	JHK
NGC 3351	SB(r)b	778	10.1	49	Ring	Starburst	06/11/95	K
NGC 3504	(R)SAB(s)ab	1539	20.5	99	Ring+spiral	Starburst	04/02/96	JHK
NGC 3516	(R)SB(s)	2649	35.3	171	Ring	Seyfert 1.5	06/11/95	JHK
NGC 3982	SAB(r)b	1109	14.8	72	Spiral	Seyfert 2	04/02/96	JHK
NGC 4303	SAB(rs)a	1566	20.9	101	Ring	Seyfert	05/02/96	JHK
NGC 4314	SB(rs)a	963	12.8	62	Ring+spiral	—	03/02/96	JHK
NGC 4321	SAB(s)bc	1571	16.1	70	Ring+spiral	—	10/06/94	K
							04/02/96	JH
NGC 5248	SAB(rs)bc	1153	15.4	74	Ring+spiral	—	04/02/96	JHK
NGC 6951	SAB(rs)bc	1424	19.0	92	Ring+spiral	LINER/Sy	26/09/94	JHK

Table 1. Properties of our sample galaxies: morphological classification (col. 2; data from de Vaucouleurs et al. 1991), velocity (col.3; data from NED, the NASA/IPAC Extragalactic Database), distance and scale (col. 4 and 5, from Ferrarese et al. 1996 for NGC 4321 and Graham et al. 1997 for NGC 3351; from the velocity and H_0=75 km s^{-1} Mpc^{-1} for all other objects), the dominant circumnuclear feature as determined from our data (col. 6), class of nuclear activity (col. 7; data from NED), date of run and passbands (col. 8 and 9). All images were obtained with MONICA on the *CFHT* except the K-image of M100, which was obtained at UKIRT (Knapen et al. 1995a).

ies. Dust lanes and nuclear rings appear to be the dominant circumnuclear features.

Dust lanes have been interpreted as the location of shocks in the gas flow. Thus, the morphology of the dust distribution can reveal characteristics of the dynamics of these galaxies (Athanassoula 1992) and of the kinematics of the gas. According to Athanassoula's models, the degree of curvature of the dust lanes is a direct indicator of the strength of the bar for bars which are not very strong. Nuclear rings, which are usually sites of active star formation (SF), occur at the location of strong density enhancements in the gas, where the bar-driven inflow of gas slows down in the vicinity of inner Lindblad resonances (ILRs; Athanassoula 1992; Heller & Shlosman 1994; Buta & Combes 1996; Shlosman 1999). SF may result from the gas becoming gravitationally unstable (Elmegreen 1994, 1997), or from triggering in miniature spiral arms (Knapen et al. 1995b, 2000).

Whereas imaging in the blue, ultraviolet, or in spectral lines like Hα traces the massive SF (e.g. Sersic & Pastoriza 1967; Pogge 1989a,b; Knapen et al. 1995a; Maoz et al. 1996; Colina et al. 1997), near-infrared (NIR) imaging offers very important advantages. Firstly, the presence of substantial and mostly unquantified amounts of extinguishing (absorbing and scattering) dust in the CNRs hampers the interpretation of imaging at especially the UV and optical wavelengths. NIR, particularly K-band, emission is much less susceptible to extinction by dust (a factor of 10 when comparing K to V), whereas colour index images such as $I-K$ (Knapen et al. 1995a) or $J-H$ are clear morphological dust indicators due to the relatively modest changes in those colours caused by different stellar populations. Secondly, NIR observations are of particular importance to the study of the CNRs because they allow a better determination of the mass distribution (excluding dark matter). NIR imaging is more sensitive to light primarily from cool giants and dwarfs which dominate the mass or are at least directly proportional to it. However, as shown in the literature and by us in this paper, there can be significant, or even dominant, contributions from young stars to the NIR emission even in the K-band, so for objects with strong SF any estimate of the mass distribution made from NIR maps must take the varying M/L ratio into account (Knapen et al. 1995a,b; Elmegreen et al. 1997; Wada, Sakamoto & Minezaki 1998; Ryder & Knapen 1999).

The atlas of images presented in this paper (Paper I) represents the first results of a programme which studies the circumnuclear structures that appear at small scales (a few hundred parsecs to a kpc) and their connection with the global disc structure in a sample of 12 barred spiral galaxies. We present J, H and K-images at subarcsec resolution for all 12 sample galaxies, and *Hubble Space Telescope* (*HST*) archive H-band images for 10 of them. In Paper II (Pérez–Ramírez & Knapen 2000a), we present an accompanying optical data set of broad-band and Hα images of the complete discs of all our sample galaxies, while in Paper III (Pérez–Ramírez & Knapen 2000b) the morphological information is interpreted in terms of the structure and evolution of CNRs of barred galaxies.

In Section 2, we describe the observations and data reduction techniques. The imaging data are presented as a series of multi-panel figures, which show broad-band images, colour index images highlighting dust and SF features against the dominant stellar luminosity, and radial profiles of ellipticity, position angle, surface brightness and colour. The results are summarized in Section 3 for individual galaxies, and briefly discussed in Section 4, while concluding remarks are given in Section 5.

2 SAMPLE SELECTION, OBSERVATIONS AND DATA REDUCTION

2.1 The sample

The main selection criterion for our sample is the presence of a bar and evidence of some circumnuclear structure associated with it, such as rings, nuclear bars or regions of SF.

Figure 1. *HST* NICMOS images of the central areas of our sample galaxies obtained using the F160W filter (comparable to H-band). The regions shown are $19''$ squared in all cases. The grey scales are stretched in such a way as to emphasize the morphology of the CNR. Only NGC 3516 is shown with a logarithmic grey scale stretch, all others linear. Black and white border regions are due to rotation of the images and the orientation of the object on the array. The orientation of the images is the same as of those in Fig. 2, i.e., N is up, E to the left.

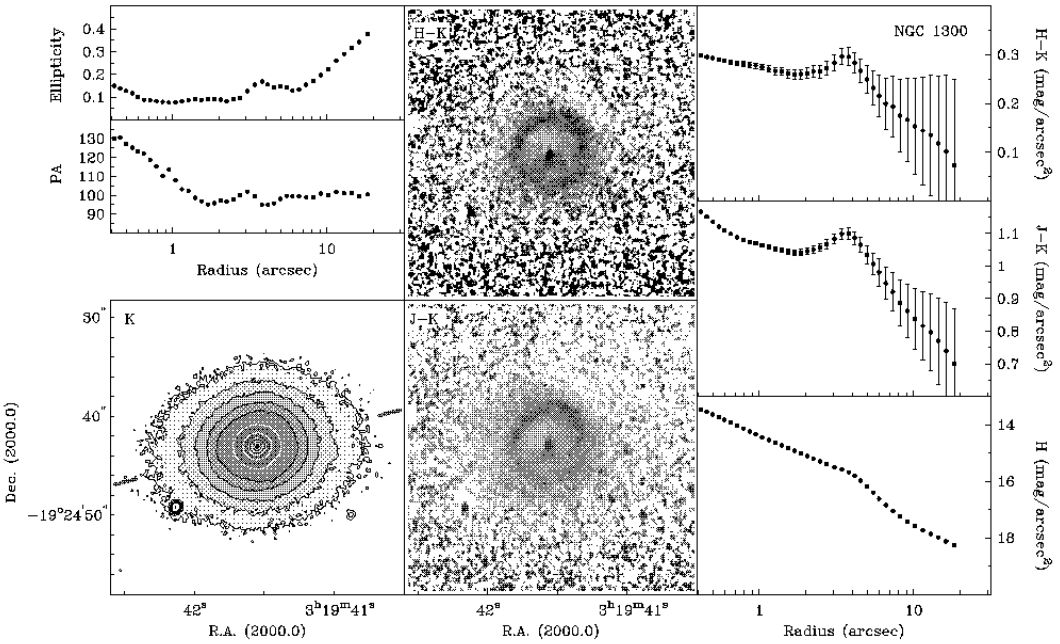

Figure 2. Images and photometric profiles for the individual galaxies. On the upper left ellipticity ($1 - b/a$) and major axis position angle (in degrees) are plotted as a function of major axis radius. The position angle has been measured from N through E. The lower left panel is a contour plus grey-scale plot of the K-band image of the galaxy. Contours start at K=17.5 mag arcsec^{-2}, with intervals of 0.5 mag arcsec^{-2}. The coordinates are J2000.0, obtained from the NASA/IPAC Extragalactic Database (NED). The orientation of the major axis of the main bar, as determined from the optical imaging in Paper II, is indicated whenever appropriate by a pair of tickmarks near the border of the lower left panel. The middle two panels are grey-scale representations of $J - K$ and $H - K$ colour index images with a grey-scale range of 0.5 mag arcsec^{-2}. Redder colours are indicated by darker shades. The right panels show the H-band surface brightness profile (bottom), and the $J - K$ (middle) and $H - K$ (top) colour profiles. The colours and the H-band surface brightness have been photometrically calibrated using aperture photometry in the literature (see Section 3). **a.** NGC 1300

Furthermore, the sample galaxies should be nearby, bright and observable from the northern hemisphere. Some of the sample galaxies are taken from the lists published by Sersic & Pastoriza (1967) and Pogge (1989a,b).

The sample can be considered more anecdotal than complete in any sense. However, it does significantly increase the sample size when compared to published NIR studies of CNRs in barred galaxies, which rarely include more than three objects and usually discuss only one (e.g. Knapen et al. 1995a,b; Elmegreen et al. 1997; Laine et al. 1999; Ryder & Knapen 1999). With our new imaging, we also improve the spatial resolution, and show different colour index maps, $J - K$ (primarily outlining dust extinction) and $H - K$ (additionally indicating the possible emission due to hot dust in the case of the more active sample galaxies). Regan & Mulchaey (1999) show *HST* 1.6μm and optical-infrared (basically $R - H$) colour index images of a sample of Seyfert (Sy) galaxies, including a number of CNR galaxies. Two of the galaxies in their sample are also included in our sample (NGC 3516 and NGC 3982). The $R - H$ colour, however, is much more sensitive to changes in stellar populations than the NIR colours used in our paper. For 10 of our sample

galaxies, we have retrieved, in addition to our own data, *H*-band images from the *HST* archive (Fig. 1), and we comment on the high-resolution NIR morphology of those objects. In Table 1 we give some information about the classification of the galaxies of our sample, the predominant circumnuclear feature, as determined from the data, and the type of nuclear activity, if known.

2.2 Ground-based observations

We have obtained NIR broad-band images in the *J* (1.25μm), *H* (1.65 μm) and *K* (2.2 μm) bands of the 12 barred galaxies that make up our sample, during three observing runs: 1994 September 26, 1995 November 5–6, and 1996 February 3–5. The observations were made with the 3.6 m Canada–France–Hawaii Telescope (*CFHT*). We used the Montreal NIR camera (MONICA; Nadeau et al. 1994), equipped with a 256 x 256 pixel HgCdTe array detector with a projected pixel size of $0\farcs248$.

Since the sky background in the NIR is bright and changes rapidly, it is essential to obtain sky frames frequently. We observed the sky usually just before and after each galaxy observation. Frames typically consisted of four co-added individual exposures. Separate frames with the nucleus of the galaxy at slightly offset positions were co-added in the reduction process to produce the final mosaic images.

The weather was clear and generally photometric thoughout these nights, and the seeing values as measured from our final images were $0\farcs7$ – $1\farcs0$.

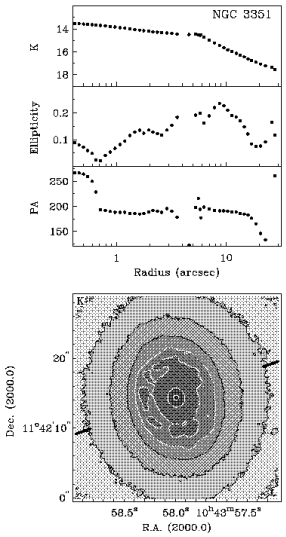

Figure 2. d. NGC 3351

2.3 Data reduction

The main steps in the reduction of the NIR data include subtracting the sky background, interpolating across known bad pixels, and registering and combining the images. The data reduction was done partly with private programmes and partly with standard IRAF routines.

We first combined four sky exposures taken at different positions on the sky immediately before and after a series of galaxy exposures by median-averaging them, while iteratively rejecting those values in the averaged sky exposure that deviate by more than 3σ from the average value in that frame. This procedure allows the automated rejection of any star images that might have been present in the sky exposures, which were observed by offsetting the telescope blindly to a position a few arcmin from the galaxy centre. We then subtracted the averaged sky image from the relevant galaxy images.

A close inspection of the sky-subtracted galaxy images of the 1996 run showed the presence of periodic, horizontal lines which could be traced back to electronic crosstalk in the system. This raises the noise level in these images. In order to correct the problem, we used a Fourier transform technique to locate the frequencies of the maximum intensity in the images, and filtered them out. This resulted in a considerable improvement in most images, although in a few images interference stripes are still notable at low levels.

After flat-fielding with dome flats, and masking the unreliable pixels in the array, we combined the sky-subtracted and, where appropriate, de-striped images. Ideally, one would like to locate one or more common field stars in the images to achieve the most accurate alignment possible. Unfortunately, the field of view of our images is small and in most cases we could only use the nucleus of the galaxy itself to determine the reference position. The individual images were thus registered and shifted to a common position (in all cases accurate to a fraction of the pixel size) and averaged. In the process, the pixel size was halved to increase sampling (reduced from $0\farcs248$ to $0\farcs124$). Finally, we rotated the images by an angle of 88.8° in order to obtain the correct north (up), east (left) orientation.

2.4 Photometric Calibration

Although we subtracted the background sky as described in Section 2.3, we cannot check on how accurate our sky subtraction is since the sky is variable, and the frame is small compared with the galaxy. This makes it very hard to estimate to what level the flux registered in the photometric aperture is influenced by any residual background emission. For that reason, we have used aperture photometry from the literature. By calibrating with multiple aperture measurements we can better estimate the value of the sky and the efficiency of the system. If only one useful aperture is available, we can use only the relatively bright part of the image. We were able to find the aperture photometry in *J*, *H* and *K*-bands for all but one of the galaxies, NGC 1530. For this galaxy, we used the average magnitude offset as determined for the rest of the galaxies. Literature photometry sources include Glass (1976), Aaronson (1977), McAlary,

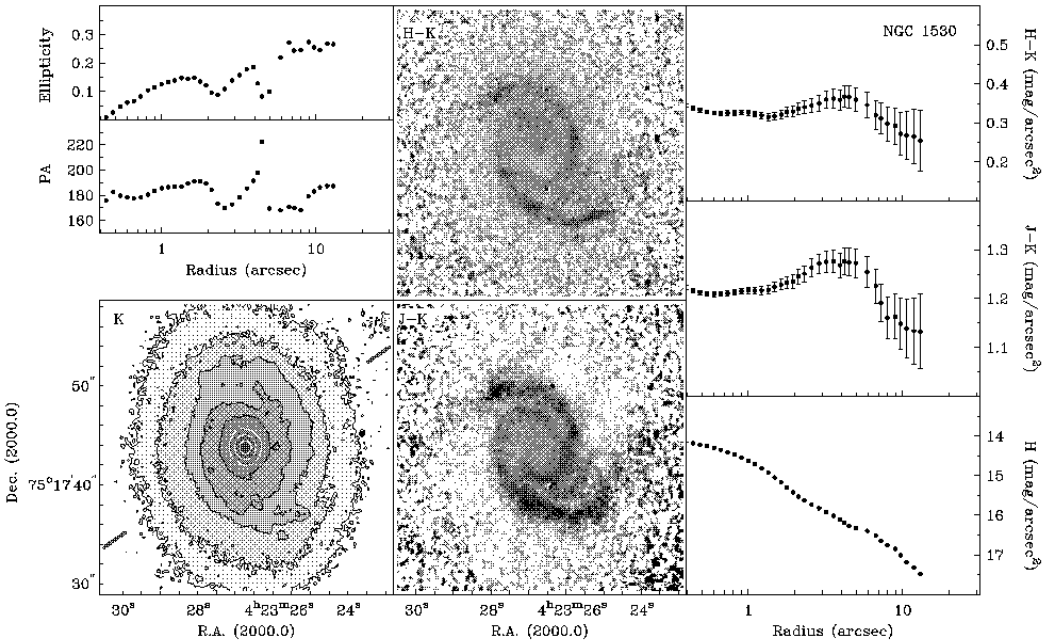

Figure 2. b. NGC 1530

McLaren & Crabtree (1979), Balzano & Weedman (1981), Willner et al. (1985) and Spinoglio et al. (1995).

To check the quality of our photometry, we also made comparisons with data from the literature. We selected values from Glass (1984), Cidziel, Wynn-Williams & Becklin (1985), Devereux, Becklin & Scoville (1987) and Hunt et al. (1994). The average absolute difference between our results and the results from different authors was 0.12 mag.

Direct comparison of the surface brightness profile in the H-band and the $H-K$ colour profile plots was possible for two of our sample galaxies, NGC 3516 and NGC 3982, which are in common with the Peletier et al. (1999) sample. The photometric calibration procedures used were slightly different, but the agreement in both cases was good.

2.5 Colour index maps and radial profiles

Colour index maps were created after assuring that the relevant pairs of images were at the same pixel scale and orientation and at comparable resolution before combining them.

After calibrating the images, we used GALPHOT (Jørgensen, Franx & Kjaergaard 1992) to fit ellipses to the images. The centre position, ellipticity and the position angle of the fitted ellipses were allowed to change freely as a function of radius for the H passband. The values for these parameters were then used as input for the fits to the images in other passbands, in order to ensure that we produce reliable colour profiles. In the case of NGC 2903, the position angle and ellipticity were kept constant because the large amount of structure present in the core did not allow a meaningful fit to these parameters. We thus produced plots (shown in Fig. 2) of the surface brightness of the H-band as a function of radius, and colour profiles in $J-K$ and $H-K$ for all the galaxies which were imaged in these bands. Errorbars in these plots indicate the uncertainty in the determination of the sky background. We have estimated these uncertainties using the procedure described by Peletier et al. (1999), where 1σ errorbars correspond to μ_H= 21.5 mag arcsec^{-2}, μ_J= 21.2 mag arcsec^{-2} and μ_K= 20.5 mag arcsec^{-2} (about 0.1% of the sky background in H and K and 0.3 % in J).

In Fig. 2, we show for each galaxy (except NGC 3351 for which we only obtained a K-band image) greyscale representations of the K broad-band and $J-K$ and $H-K$ colour index images, radial profiles of position angle and ellipticity as determined from the fit to the H-band image (K for NGC 3351), and radial surface brightness (H) and colour ($J-K$ and $H-K$) profiles. We tabulated the values plotted as a function of radius, but publish the tables in electronic form only‡. They are also available from the authors.

‡ The data tables are available electronically from the Centre de Données astronomiques de Strasbourg (CDS), on: ftp://cdsarc.u-strasbg.fr/pub/cats/J/MNRAS/volume/first_page .

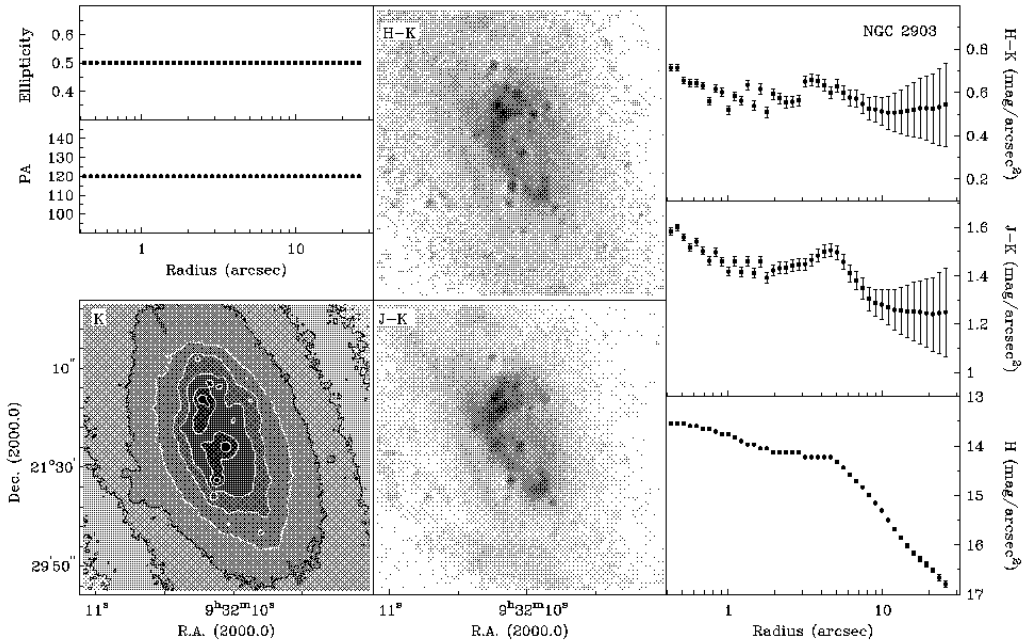

Figure 2. c. NGC 2903, ellipticity and position angle were fixed in the fitting process

2.6 *HST* NIR imaging

For 10 of our 12 sample galaxies, NICMOS imaging with the *HST* is available from the *HST* archive. We retrieved the re-reduced F160W (comparable to H-band) images from the archive. However, we improved the quality of some of these images by doing additional data reduction to remove artifacts. We relied on header information to place the images on an astrometrically correct grid. The images are all taken with the NIC2 camera, with a pixel size of $0\farcs075$. In most cases, the image retrieved from the archive is a combination of several individual exposures. For NGC 3516 and NGC 3982, however, one single exposure was available, and these images in fact improved most due to our additional data reduction. Regan & Mulchaey (1999) published two of these images (NGC 3516 and NGC 3982). We show the central areas of all images in Fig. 1, with the same scale and orientation. In most of the objects, a wealth of detail can be seen in the CNR. The emission usually coincides with the location of the SF ring, and most of the individual bright knots are due to regions of current SF. Dust lanes and/or SF regions often outline spiral-like patterns, which will be discussed in more detail below, and in Paper III.

3 RESULTS ON INDIVIDUAL GALAXIES

In this section, we describe some of the results of the NIR imaging of our sample galaxies, as shown in detail in Fig. 1 (*HST* NIR images) and Fig. 2 (ground based multi-band images and profile fits). A more systematic study of parameters derived from these data in combination with optical imaging of the complete galaxy discs is forthcoming (Papers II and III).

3.1 NGC 1300

Our broad-band NIR images are remarkably smooth, and do not show any structure in the CNR (Fig. 2a). The colour index images, however, show a red ring-like structure, possibly outlining a single spiral arm that departs from the nucleus towards the west side of the image and continues to wrap around the nucleus until it closes in a ring. This ring appears more continuous and broader in the northern part than in the south where it looks patchy. The feature seen in our NIR colour index map cannot be an artifact of combining two images with slightly different spatial resolution, because such an artifact would show up as a complete ring, whereas the observed red feature is not at constant galactocentric radius. Pogge (1989a) saw an incomplete nuclear ring in Hα emission with a number of distinct "hot spots".

The *HST* H-band image resolves the nuclear ring into

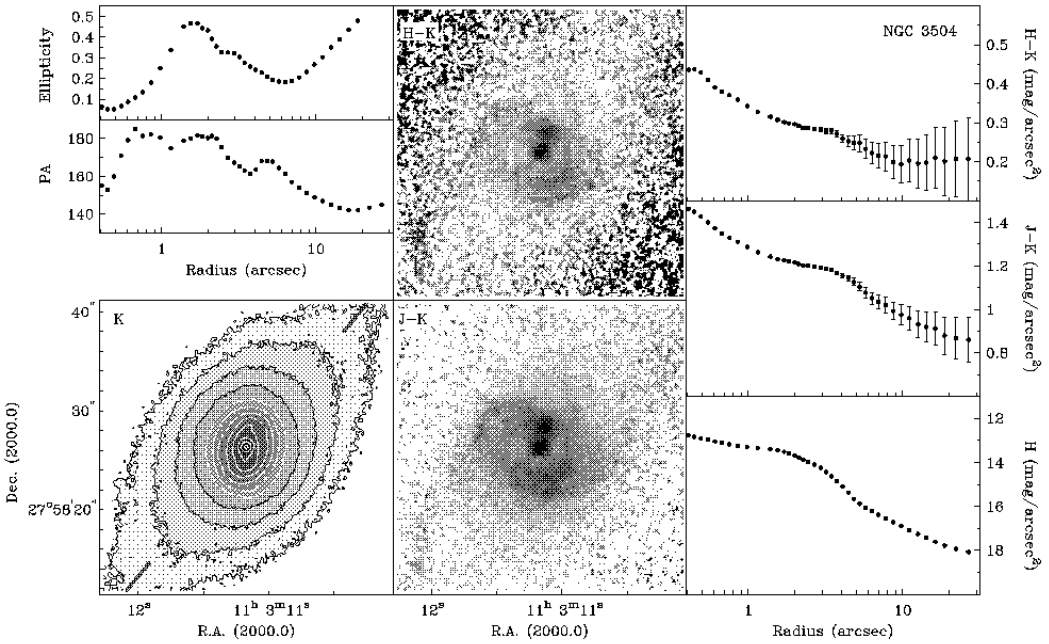

Figure 2. e. NGC 3504

a series of tightly wound spiral armlets, outlined in dust and stellar populations. The ring region is of a relatively low amplitude compared to the central bulge component, in contrast to nuclear rings in other objects, e.g. NGC 3351, as can be observed in Fig. 1.

The location of the ring corresponds to a bump in all radial profiles (i.e., surface brightness, colour, ellipticity and position angle). The $J-K$ colour of the ring is redder by 0.1 magnitudes than the background. No isophotal twists are seen in the ellipticity and position angle profiles or in the contour map of the K-band image. Thus we confirm that there is no evidence for a nuclear bar (Regan & Elmegreen 1997).

3.2 NGC 1530

We find very well-defined mini-spiral structure in the central region of this galaxy (Fig. 2b). Reynaud & Downes (1997; see also Reynaud & Downes 1998, 1999) suggest that the molecular gas distribution in the central 5 kpc of this galaxy is concentrated along arc-like shock features. Our $J-K$ image shows that these arcs are part of a well-defined nuclear spiral structure. Furthermore, Reynaud & Downes suggest that a patchy molecular ring may lie inside these shock fronts, possibly connected to them. Fig. 2b reveals that the spiral structure forms a pseudoring around the nucleus. Even the broad-band image shows considerable structure in the CNR. No isophote twists can be seen in the position angle plot. Distinct regions, presumably of enhanced SF, can be noticed along the mini-spiral in the broad-band NIR images. These regions coincide in position with the dark (red) lanes seen to outline the mini-spiral in the $J-K$ image. This implies that the mini-spiral in $J-K$ is not necessarily a dust spiral (as would have been tempting to conclude from the colour index image alone) but may well be delineated by either emission from young stars (e.g. red supergiants), or from hot dust. We conclude that we see a mini-spiral in the NIR, outlined by emission from SF and dust. This mini-spiral is well traced also on the *HST* H-band image (Fig. 1) as a collection of distinct luminous regions outlining the armlets, which are accompanied by dust lanes.

Like in the case of NGC 1300, a bump in the radial profiles is visible at the location of the ring. The $J-K$ colour of the ring is 0.05 magnitudes redder than the background colour. No pronounced change of slope is detected in the H-band surface brightness profile, which overall decreases more smoothly than in the other galaxies discussed here.

3.3 NGC 2903

Fig. 2c shows several peaks of SF in the CNR of this starburst galaxy, which, as expected, are resolved in much more detail in the *HST* NICMOS image we obtained from the *HST* archive (Fig. 1). These peculiar 'hot spots' in the nu-

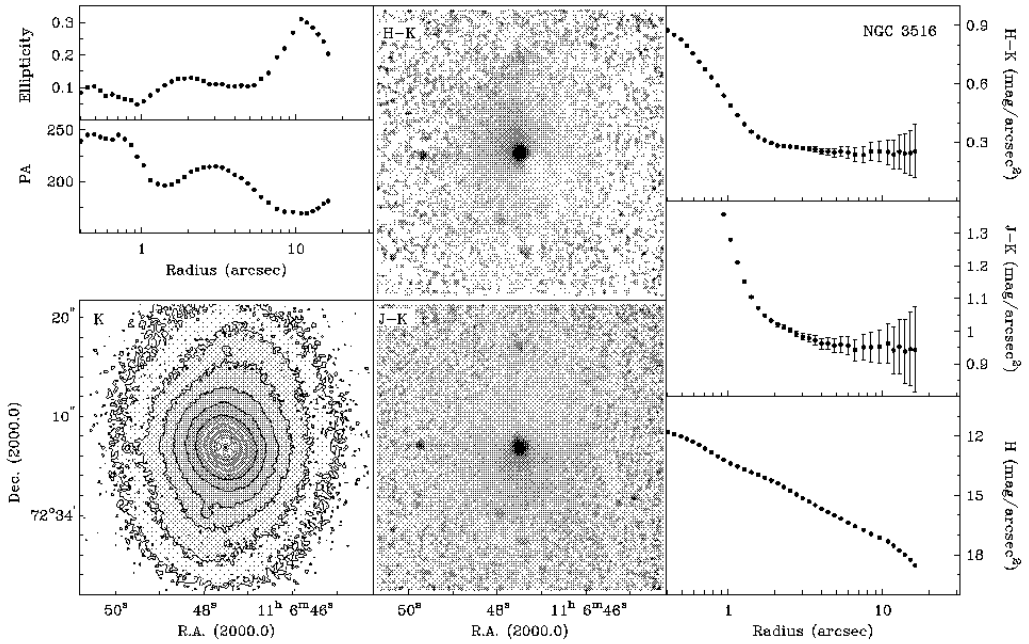

Figure 2. f. NGC 3516

clear region have been identified and described in different ways by various authors. Marcelin, Boulesteix & Georgelin (1983) found six 'hot spots' forming a linear structure that crosses the central region. A later study in infrared and radio by Wynn–Williams & Becklin (1985) showed that bursts of SF were not confined to the visible hot spots. Simons et al. (1988) noticed the presence of organized dust structure in the CNR using NIR and optical imaging. We see patches of dust in our images, but no coherent structure.

Regan & Elmegreen (1997) found that this galaxy has an isophotal twist, using a K-band image of the inner bar region, although the results from an earlier study by Elmegreen et al. (1996) were ambiguous. Similar twists have been interpreted as nuclear bars or triaxial structures (e.g., Shaw et al. 1995; Friedli & Martinet 1993; Wozniak et al. 1995). However, our images show such an abundance of structure that it is hard to imagine that the measured changes in the radial behaviour of ellipticity or PA would have any significance in this respect. For that reason, we set the ellipticity and the PA to fixed values corresponding to the parameters of the isophotes on the outskirts of our images when we fit our radial colour profiles.

As in, e.g., NGC 1300, the circumnuclear ring-like region of enhanced SF shows up in the surface brightness profile as a change of slope, and in the colour profiles as a significant red bump at the same radius.

Our colour index maps suggest that the nuclear hot spots may be part of a pseudoring. We can identify more than six clumps in the broad-band images, and even more in the colour index map. This is in good agreement with the idea that obscuration by dust is the reason for a previous underestimate of the extent of this SF region (cf. Jackson et al. 1991). As in NGC 1530, we see significant emission from SF regions in the NIR, including the K-band, which must at least in part be due to red supergiant emission. The red $J-K$ and $H-K$ colours of these regions makes them stand out clearly in the colour index maps.

3.4 NGC 3351

We only obtained a K-band image (Fig. 2d), which shows an incomplete ring of presumably SF clumps. The *HST* H-band image (Fig. 1) shows the same ring but at significantly higher resolution, and resolved into a large number of individual luminous regions, presumably star-forming. Some of the brightest knots can be recognised in the UV (~ 2200Å) *HST* image published by Colina et al. (1997), but others, e.g. the one north of the nucleus, are absent from the UV image. Dust extinction is the most likely candidate mechanism for this absence, although stellar population differences can be envisaged as culprits as well. Spiral arm structure is not obvious in the CNR, and if it is present at all it is very tightly wound. There is only little evidence of dust organised into lanes, and the best example of such a dust lane is

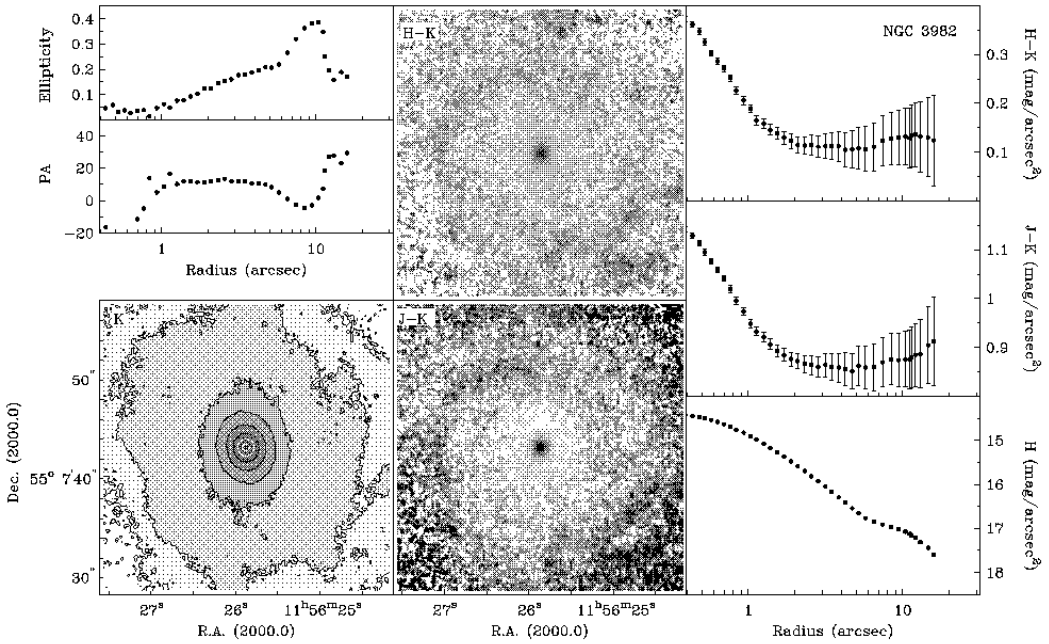

Figure 2. g. NGC 3982

seen towards the south-east in the *HST* image. In contrast, and as a direct result of their much lower spatial resolution, Shaw et al. (1995), found evidence for a circumnuclear ring only in their $J-K$ colour map.

As in the other galaxies discussed before in this section, there is a dichotomy in the slope of the K-band surface brightness profile. The change occurs at the radius of the SF "ring", and can be explained as the transition between an inner active SF region and the quiescent disc around it. PA and ellipticity are difficult to fit in that area, but their radial profiles show consistent behaviour in- and outside the nuclear ring.

3.5 NGC 3504

Our NIR imaging of this barred galaxy reveals a lot of structure, including a double peak in the central part of the NIR broad-band images (Fig. 2e). Recent adaptive optics images obtained with the *CFHT* (by F. Combes & J.H. Knapen, private communication) confirm this double peak, but spectroscopic follow-up observations are needed to confirm whether these peaks are in fact two nuclei. No *HST* NIR imaging is available.

The colour index images show a pair of long and straight dust lanes that come into the CNR through the main bar, and intricate dust lane structure in the central region. The nuclear double peak is very obvious in the colour index maps. Elmegreen et al. (1997) showed a ring in $J-K$ with five discrete clumps of SF. The signal to noise ratio in our images is too low to reveal these SF clumps.

The previously reported isophote twist (e.g., Pompea & Rieke 1990) is obvious from our imaging, as well as from the PA and ellipticity profiles. The double bar, outlined by the two separate peaks in the ellipticity profile, is most probably not exclusively due to the nuclear double peak, because the accompanying isophote twist in fact starts somewhat outside the region of influence of the double peak. The surface brightness and colour profiles show the hump at the CNR radius that is seen in many similar galaxies presented in this paper.

3.6 NGC 3516

The only obvious feature in our images is the very red nucleus. Neither the broad-band *HST* H-image, nor our ground-based NIR colour maps reveal any other structure (Fig. 1, 2f). Regan & Mulchaey (1999) used an *HST* WFPC2–NICMOS colour index map to show that a single spiral dust pattern dominates the circumnuclear morphology of this galaxy. They described a strong red dust lane that emerges from a blue feature north of the nucleus at a radius of 3″. The spatial resolution of our images is not high enough to reveal such fine details. The differences between our images and *HST* images are probably due to the longer

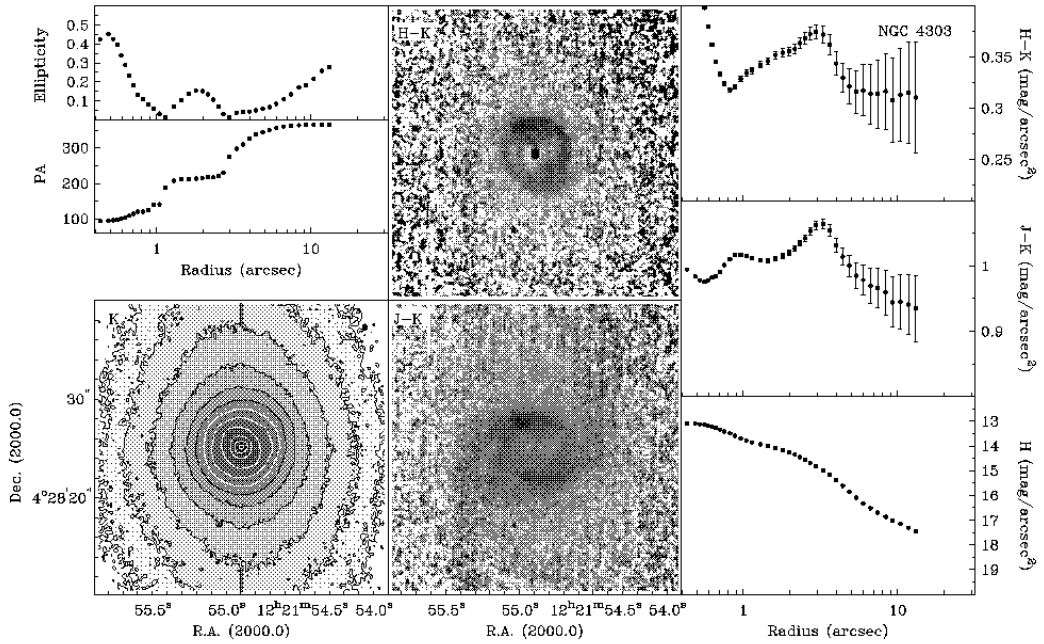

Figure 2. h. NGC 4303

spectral baseline that Regan & Mulchaey used (0.55 μm to 1.6 μm) and the different spatial resolution.

Quillen et al. (1999) noticed that the inner J-band isophotes are slightly elongated in a direction roughly perpendicular to the outer bar, so the galaxy may be doubly barred. Our H-band profile indeed shows an isophote twist of about 50° (Fig. 2f). Quillen et al. (1999) saw a curved dust feature at about 4 arcsec south of the nucleus in their *HST* WFPC2–NICMOS colour index map.

3.7 NGC 3982

We see a multi-armed spiral pattern in our images (Fig. 2g), in agreement with Regan & Mulchaey (1999) who describe the global morphology of this galaxy as multi-armed. There is a lot of structure in our ground-based images, but a detailed comparison with the colour index maps obtained by Regan & Mulchaey (1999) is difficult due to the lower spatial resolution of our images. The *HST* NIR image (Fig. 1) is the one used by Regan & Mulchaey, and shows the rather faint spiral structure in the CNR. Our colour index map shows that this galaxy has a small red nucleus, classified as Sy2. The ellipticity of the isophotes reaches a maximum at a radius of 9 arcsec. This could correspond to a ring, a small bar or a triaxial bulge.

The radial colour profiles ($J-K$ and $H-K$) follow a characteristic shape, becoming very red close to the nucleus, with the colour most likely due to emission from dust heated by the AGN radiation field. The colours become bluer until a certain radius (the location of the ring), after which they remain constant. Such a profile shape is only seen in the AGNs of our sample. The difference in colour between the nucleus and the ring radius is about 0.2 magnitudes in both $J-K$ and $H-K$.

3.8 NGC 4303

Buta & Crocker (1993) classify this galaxy as having a nuclear ring, based on their Hα data. Elmegreen et al. (1997), using NIR observations, did not detect any ring. According to them, the ring consists of very young stars which do not show up in the NIR. However, we can see a well-defined ring in our $J-K$ and $H-K$ images (Fig. 2h). There is a pair of dust lanes which connect the bar to the nuclear ring in the south and north. The reddest colours are seen where the dust lanes merge with the nuclear ring.

Colina et al. (1997) present a UV ($\sim$ 2200Å) *HST* image of the CNR of NGC 4303, which shows spiral structure outlining massive SF, continuing all the way into the unresolved core on the NE side of the nucleus. The UV SF spiral is strongest on the side opposite to where we see the largest concentrations of dust (darkest patches in Fig. 2h) in our NIR colour index maps. Our *HST* H-band image shows

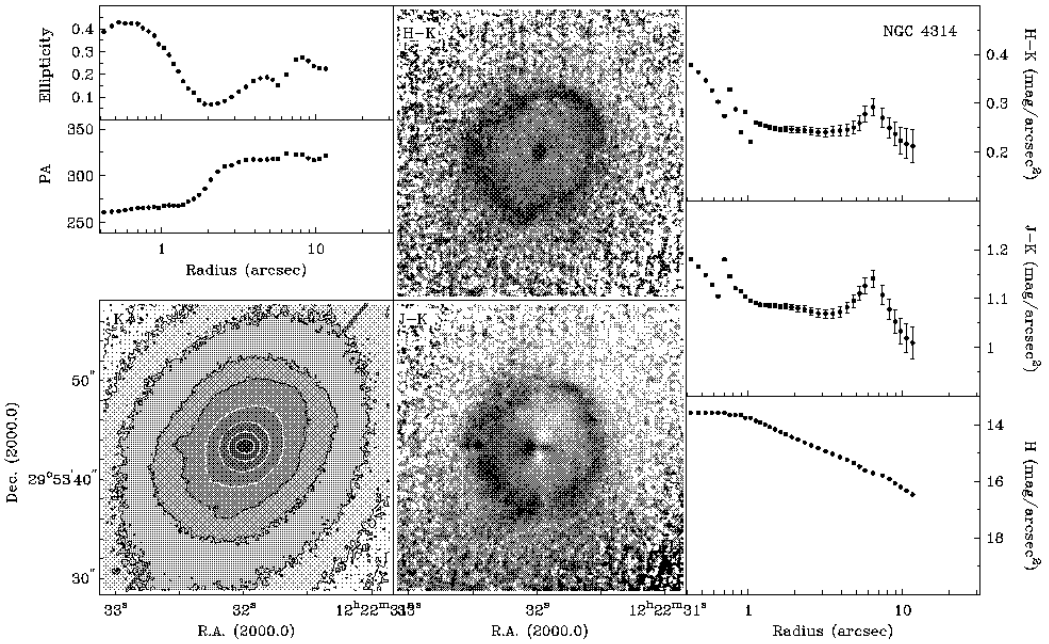

Figure 2. i. NGC 4314

some spiral structure in the NIR but emission is dominated by the central bulge component.

There are strong isophotal twists within the central 7 arcsec, and a possible nuclear bar with a radius of 2 arcsec where the ellipticity reaches a peak of 0.2 and the position angle is constant at about 220°. The signature of the ring can be recognised as a red peak in the $J-K$ and $H-K$ colour profiles, as well as in all other profiles.

3.9 NGC 4314

Our ellipticity and PA profiles provide some evidence for a nuclear bar with a radius of 1–2 arcsec. The corresponding PA twist can be recognized in the contours of the broad-band image. Benedict et al. (1993), using the WFPC camera on the *HST*, found an oval distortion with a length of 8 arcsec in the nuclear region. Wozniak et al. (1995) suggested that this galaxy could be another example of a double-barred galaxy, although they found it difficult to confirm this with their ground-based image at a considerably lower spatial resolution than our new data.

The colour maps published by Shaw et al. (1995) revealed the presence of the circumnuclear ring, which is so prominent in the optical (e.g., Morgan 1958), and especially in Hα (e.g., Pogge 1989a). This ring is redder than all the other regions in the galaxy, having colours consistent with those of typical old stellar populations in ellipticals and spiral bulges. We see a smooth and continuous ring in our $J-K$ colour index map (Fig. 2i). The *HST* H-image (Fig. 1) shows a wealth of emitting structure in narrow tightly wound spiral armlets in the nuclear ring. Fine dust lanes are seen to accompany the spirals. The radial profiles also show the signature of the ring, most clearly with colours that are about 0.1 magnitude redder than the background.

3.10 NGC 4321

The prominent star-forming CNR of NGC 4321 (M100) has been studied in great detail using, e.g., optical and NIR imaging, CO interferometry, and modelling (e.g., Pogge 1989; Knapen et al. 1995a,b; Knapen 1998; Wada et al. 1998; García–Burillo et al. 1998; Ryder & Knapen 1999; Knapen et al. 2000). Knapen et al. (1995b) concluded that M100 has a circumnuclear starburst maintained by a global bar-driven density wave.

As already shown in detail by Knapen et al. (1995a), the K-image of this region is generally smooth, in contrast to the appearance in optical and Hα. Two symmetrically placed 'hot spots', named K1 and K2, are obvious in Fig. 2j, both in emission in the broad-band image, and as red features in the colour index images. Ryder & Knapen (1999) recently used NIR imaging and spectroscopy to confirm the suspicion that K1 and K2 are in fact regions of enhanced SF, and the K emission from those regions is partly due to young

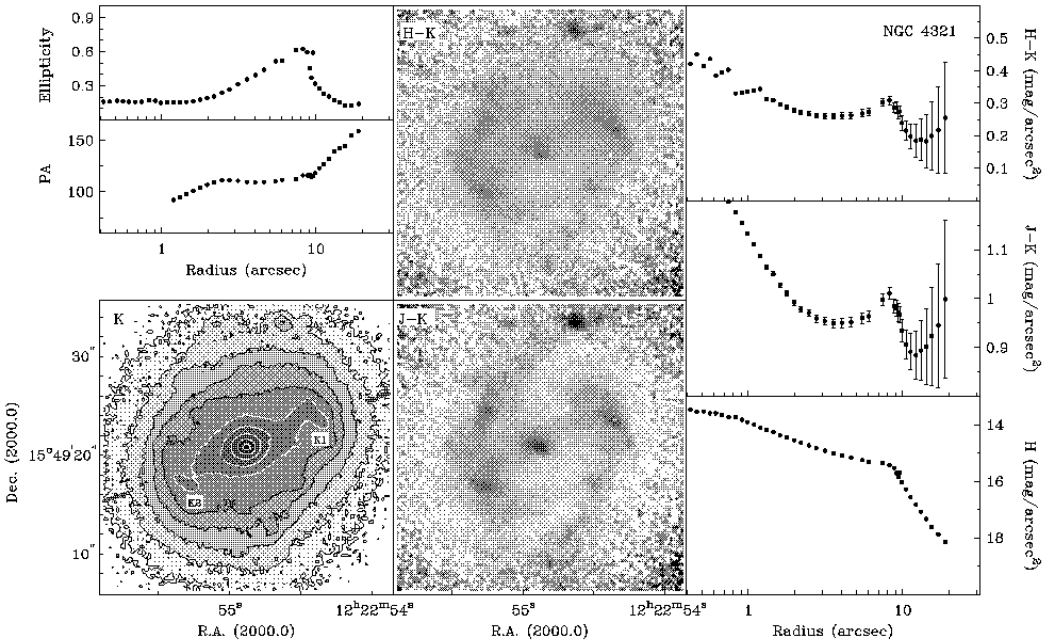

Figure 2. j. NGC 4321

stars (Knapen et al. 1995a,b). Our NIR imaging confirms the location of dust lanes and suspected SF regions, shown by Knapen et al. (1995a) in their $I-K$ colour index map. The locus of the circumnuclear ring-like structure shows up prominently in all radial profiles. Unfortunately, no *HST* NIR images are available.

3.11 NGC 5248

NGC 5248 is a galaxy with an HII nucleus and a lot of SF activity in the CNR. Elmegreen et al. (1997) found very conspicuous central spiral arms, and several hotspots that form a ring-like spiral pattern. Buta and Crocker (1993) detected a nuclear ring with a diameter of 10–17 arcsec. This activity shows up clearly in our broad-band NIR images, as well as in our colour index maps (Fig. 2k). Spiral structure with star-forming arms, accompanied by dust lanes, is the dominant feature. The western spiral arm has colours which are redder by about 0.1 mag in $J-K$ than its counterpart in the east. Our $J-K$ image has been published earlier by Laine et al. (1999). They compared it with the images obtained using adaptive optics, which show a nuclear grand-design spiral structure. This nuclear spiral, at scales of tens of pc, is not expected to show up in a single broad-band NIR image, even at *HST* resolution, and in fact does not show up (Fig. 1). The *HST* H-band image does show a wealth of structure in the CNR, again in the form of emitting regions distributed along spiral arm fragments, and accompanied by less luminous regions which may well be dusty.

As in other galaxies, we can see the signature of the ring as a peak at a radius of ~ 7 arcsec in all radial profiles. There is no evidence for nested bars.

3.12 NGC 6951

The dust structure in the circumnuclear ring is the most conspicuous feature in our $J-K$ colour index map, but the star-forming regions in the ring can also be seen in the broad-band images (Fig. 2l). The bar dust lanes connect to this nuclear ring in the northeast and southwest. Several sites of SF are located along the ring, and its presence is also seen in the ellipticity and PA profiles, as well as in all other profiles (Fig. 2l).

We can also see a blue ring at about 2 arcsec, within the red nuclear ring surrounding it. This blue ring shows up as a dip in the $J-K$ profile. Its nature is not clear, and needs further study. The *HST* H-band image, used also by Pérez et al. (2000), shows a picture also seen in, e.g., NGC 3351 and NGC 4314, namely of bright emitting knots distributed along tightly wound spiral armlets in the nuclear ring, accompanied by dust lanes.

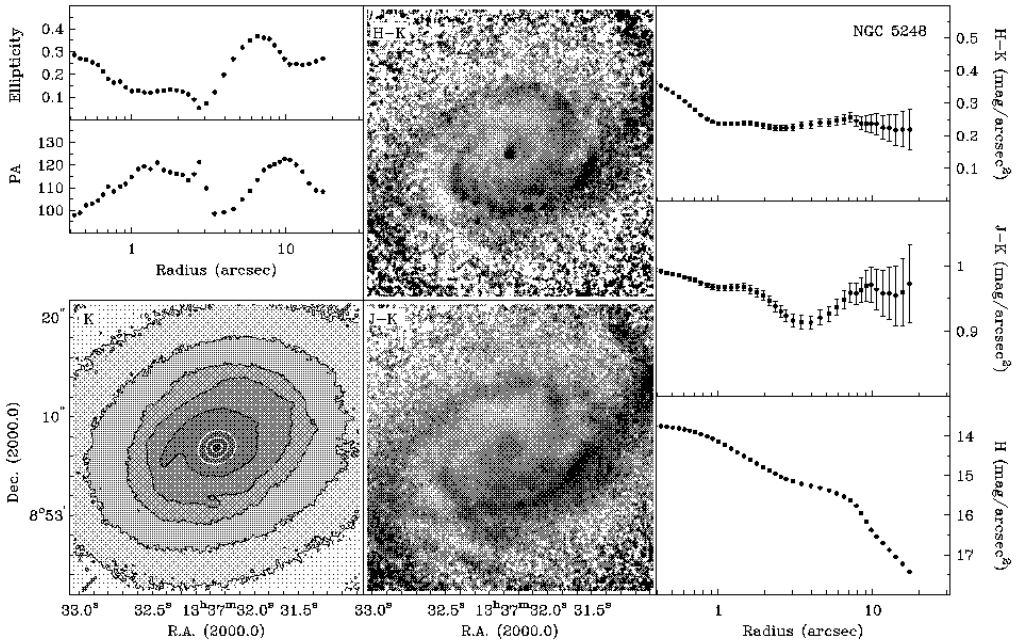

Figure 2. k. NGC 5248

4 DISCUSSION

We have presented examples of circumnuclear rings and dust lane patterns in the CNRs of a dozen barred galaxies. In most galaxies, rings are well defined, in others, nuclear spirals with different curvature radii are a predominant circumnuclear feature. There are also some galaxies where both features coexist. Our sample is composed of 12 galaxies, most of which have nuclear rings. Six of them also have clear nuclear mini-spirals (NGC 1530, NGC 3504, NGC 4314, NGC 4321, NGC 5248 and NGC 6951), while in a few others there is less clear or circumstantial evidence for mini-spirals.

4.1 Circumnuclear Rings

Simulations (e.g. Athanassoula 1992; Byrd et al. 1994; Heller & Shlosman 1994; Knapen et al. 1995b; Piner, Stone & Teuben 1995; see also review by Shlosman 1999) have shown that circumnuclear rings can arise as a consequence of bar-driven inflow and the existence of dynamical resonances in the bar. Shocks form in the gas in regions of orbit crowding along the leading edges of the bar, and dense gas accumulates in these regions. In the shock region the gas loses angular momentum through torques exerted by the bar, and flows inward. The pattern of the gas flow can be quite complex, but if two ILRs are present, inflowing gas accumulates in a ring between them (reviewed by Shlosman 1999). If there is no ILR, the gas may continue to flow inward, resulting in a nuclear starburst rather than a ring (Telesco, Dressel & Wolstencroft 1993). Other mechanisms for the origin of circumnuclear rings that have been put forward as possible origins include shear in the differentially rotating disc (Buta & Combes 1996), supermassive black hole binaries (Taniguchi & Wada 1996), and minor mergers (Taniguchi 1999).

Our sample galaxies were selected to have some kind of circumnuclear structure, and except in NGC 3516 and NGC 3982, all have clear circumnuclear star-forming ring-like regions. SF is visible in most galaxies in the high-resolution *HST* NICMOS images (Fig. 1), and also in a number of galaxies in the ground-based images. However, in all galaxies with circumnuclear SF, dust lane structure outlining small-scale spiral arms is present, as can be seen in the colour index maps (Fig. 2). This is true even for NGC 1300 where the SF regions are conspicuously absent from our ground-based NIR data and very weak in *HST* NIR images. We conclude that in this class of barred galaxies with circumnuclear SF, dust lane structure in the CNR is always direct evidence of the accompanying SF, which may also show up in broad-band NIR imaging.

NIR data are not optimal for determining the sizes of the circumnuclear features, and we will come back to this issue in future papers, where Hα imaging will be used to localize the SF activity in the CNR. However, the radial

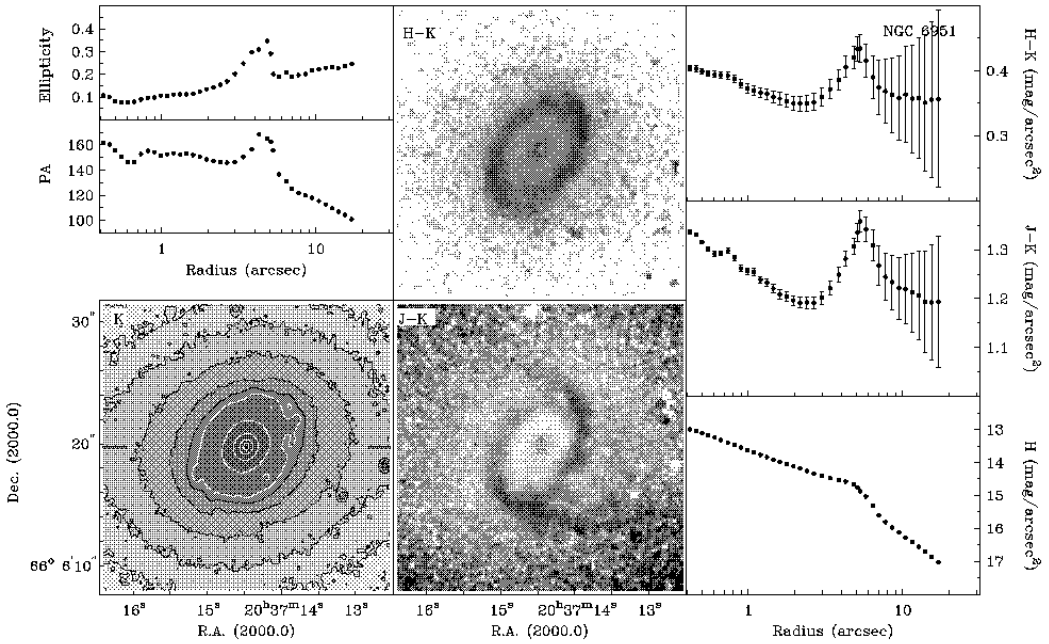

Figure 2. l. NGC 6951

profiles often allow the determination of the diameter of the "rings": typical major axis diameters are 1-2 kpc.

4.2 Dust Lanes

The first suggestion about the link between dust lanes and shocks in the gas flow was made by Prendergast (1962). Gas can follow simple periodic orbits that do not intersect when the bar or oval distortion is not very strong. When the bar is strong, the families of periodic orbits intersect and shocks are formed (e.g. Sanders, Teuben and Van Albada 1983).

Dust lanes in bars, as described by Athanassoula (1992), can be:

(i) straight and parallel to the bar major axis, or
(ii) curved and have their concave sides towards the bar major axis.

The detailed shape of the loci of offset shocks changes with the parameters of the potential (Athanassoula 1992). The simulations presented by Athanassoula show that there is a very clear sequence of shapes for the shock loci. For axial ratios corresponding to fat bars or ovals, and presumably to what could theoretically be called a weak bar, the shock lanes are curved with their concave parts towards the bar major axis. For slim ("strong")bars, the dust lanes straighten out, their curvature decreases and their shape becomes gradually more straight. For even higher axial ratios the shock loci tend towards the bar major axis. Thus, strong bars should have straight dust lanes, while ovals or weak bars should have more curved dust lanes.

Athanassoula (1992) also proposed that the strength of SF near the dust lanes depends on the strength of the bar. The dust lanes observed on the leading edges of most bars with high ellipticity (strong) are very smooth and show no HII regions or other signs of recent SF. In the case of curved dust lanes strings of HII regions are accompanying the dust lanes. Due to the enhanced gas mass fraction, dust is expected to be prominent in the CNRs themselves, and this, in fact, is seen clearly in most cases in the colour index images, and also often in the broad-band images, especially the *HST* NICMOS images. Such dust lanes are expected to be continuations of the dust lanes in the bar, and this is what is seen in our images (see Shlosman 1999 for a theoretical review).

NIR colour index images are not very sensitive to changes in stellar populations, and can outline dust structure clearly (see e.g. the $I-K$ map of M100 in Knapen et al. 1995a). We see clear and abundant observational evidence for dust lanes on several scales, but most clearly in the CNRs. Dust lanes in the bars are not well visible in general in our NIR imaging due to the lower signal to noise ratios achieved in the bar regions. In Paper II, we present optical colour index maps which outline the dust lane structure in the bars and discs of our sample galaxies more clearly,

and we study the relationship between the shape of the dust lanes, the axial ratio, and the SF in the bar in more detail.

4.3 Colour Distributions

Our colour maps have shown the presence of circumnuclear rings in most of the galaxies in our sample. These rings are generally redder than other regions in the galaxy by about 0.05– 0.1 magnitude in $J-K$ and $H-K$. From the colour index maps or colour profiles alone it is not possible to make meaningful statements about quantities of extinguishing dust implied by the redder colours. In fact, there are indications from both optical and NIR imaging and spectroscopy that the red colours in CNRs in galaxies like the ones studied here may be influenced by young stars, e.g. red supergiants (Knapen et al. 1995a,b; Knapen 1996; Elmegreen et al. 1997; Ryder & Knapen 1999). In Paper III, we will compare the precise location of the $J-K$ and $H-K$ features with those of SF regions as seen in Hα emission, and try to place quantitative limits on the origins of the red light in the CNRs.

Two of the host galaxies of Sy nuclei (NGC 3516 and NGC 3982), which have colours consistent with those measured by Peletier et al. (1999), also show a peculiar shape in the colour profiles, starting from a very red value and steeply decreasing until the radius of the ring, remaining constant afterwards. Peletier et al. (1999) suggested that the red $H-K$ (or $J-K$) colours in the cores of many Sy galaxies could be due to a significant fraction of thermal radiation from hot dust heated by the Sy nucleus. However, the two other AGN hosts in our sample (NGC 4303 and NGC 6951) do not show significantly red nuclei.

4.4 Radial profiles

One of the main data products presented in this paper is a set of detailed radial profile fits to the NIR images. We present (Fig. 2a-l) radial profiles of ellipticity, major axis position angle, NIR colour, and H-band surface brightness. We will discuss the existence and properties of (primary and secondary) bars in Paper II, where we combine the NIR profiles presented here with I-band profiles of the complete discs, covering also the primary bar, if present. Certain aspects of the radial profiles have already been discussed in Section 3, but there is one characteristic which is worth mentioning here. Apart from NGC 3516 and NGC 3982, the radial profiles show characteristic behaviour near the radius of the circumnuclear "ring". In seven (out of 10) galaxies, *all* profiles (surface brightness, colour, ellipticity and position angle) show either a change in slope, where the surface brightness profile becomes steeper, or a bump, when the colour profile shows a limited redder region caused by either dust or SF in or near the ring – see Section 4.3. These characteristics are accompanied by some change in ellipticity and position angle. In a further two galaxies (NGC 1530 and NGC 4314) only the surface brightness profile does not follow this trend, whereas in NGC 5248 the colour profile is the deviant one. Of course in NGC 2903 and NGC 3351 we cannot judge the behaviour of ellipticity/position angle and colour profiles, respectively.

We postulate that the features in the surface brightness and colour profiles are due directly to a relatively young population. Firstly, an old, bulge-like, population would not be expected to give rise to strong high-resolution features such as the ones discussed here. Secondly, if the red bumps in the colour profiles were due to extinction by dust only, they should be accompanied by relative dips in the corresponding surface brightness profiles (such dust would remove light in each of the J, H and K-bands). Instead, red bumps in the colour profiles are in all cases accompanied by bumps in the surface brightness profiles: relative excesses in emission, red in colour, that are naturally explained by excess emission produced locally by relatively young stars, probably accompanied by dust. We will come back to this issue in Paper III, where we combine the NIR data with Hα imaging.

5 CONCLUSIONS

This is the first paper in a series exploring the relationships between ring-like star-forming regions in the central few kpc regions of barred galaxies and the morphological properties of their hosts. In this paper, we present new sub-arcsec resolution NIR images obtained with the *CFHT* of the central regions of a sample of 12 barred galaxies with circumnuclear SF activity, and *HST* archival NIR images of most of the sample objects. In Paper III, we will combine these data with optical imaging of the complete hosts, as presented in Paper II.

Our NIR images reveal a wealth of structure, caused by young stars and dust. In colour index maps, structures such as SF sites and dust lanes are generally apparent, even in those galaxies where the broad-band images appear featureless. The colour maps of most galaxies show evidence of an often tightly wound spiral structure. In some cases, this spiral structure is visible also in the broad-band images, and as expected due to the higher spatial resolution, more often so in the *HST* than in the ground-based images. Where circumnuclear structure is visible in the *HST* images (in about three quarters of all cases), it shows large numbers of small emitting regions, presumably SF regions, often outlined in spiral arm fragments, and accompanied by dust lanes. Circumnuclear spiral structure thus appears to be common in barred spiral galaxies with circumnuclear SF.

In most of our sample galaxies, and in all those where the star-forming nuclear ring is well defined, radial profiles of surface brightness, colour, ellipticity and position angle show a characteristic bump or change in slope at the radius where the circumnuclear ring is located.

Acknowledgements This research has made use of the NASA/IPAC Extragalactic Database (NED) which is operated by the Jet Propulsion Laboratory, California Institute of Technology, under contract with the National Aeronautics and Space Administration.

REFERENCES

Aaronson M., 1977, PhD thesis, Harvard Univ.
Athanassoula E., 1992, MNRAS, 259, 345
Balzano V. A., Weedman D. W., 1981, ApJ, 243, 756
Benedict G. F., Higdon J. L. et al., 1993, AJ, 105, 1369
Buta R., Combes F., 1996, Fund. Cosmic Phys., 17, 95
Buta R., Crocker D. A., 1993, AJ, 105, 1344
Byrd G., Rautiainen P., Salo H., Buta R., Crocher D. A., 1994, AJ, 108,476

Cizdziel P. J., Wynn–Williams C. G., Becklin E. E., 1985, AJ, 90, 731
Colina L., García–Vargas M. L., Mas–Hesse J. M., Alberdi A., Krabbe A., 1997, ApJ, 484, L41
Devereux N. A., Becklin E. E., Scoville N., 1987, ApJ, 312, 529
de Vaucouleurs G., de Vaucouleurs A., Corwin H. G. Jr., Buta R. J., Paturel G., Furgue P., 1991, Third Reference Catalogue of Bright Galaxies. Springer, New York (RC3)
Elmegreen, B.G., 1994, ApJ, 425, L73
Elmegreen, B.G., 1997, Rev. Mex. Astr., 6, 165
Elmegreen D. M., Chromey F. R., Santos M., Marshall D., 1997, AJ, 114, 1850
Elmegreen D. M., Elmegreen B. G., Chromey F. R., Hasselbacher D. A., Bissell, B.A., 1996, AJ, 111, 1880
Ferrarese, L. et al. 1996, ApJ 464, 568
Friedli D., Martinet L., 1993, A&A, 277, 27
García–Burillo S., Sempere M. J., Combes F., Neri R., 1998, A&A 333, 864
Glass I. S., 1976, MNRAS, 175, 191
Glass I. S., 1984, MNRAS, 211, 461
Graham J.A. et al., 1997, ApJ 477, 535
Heller C. H., Shlosman I., 1994, ApJ, 424, 84
Hunt L. K., Zhekov S., Salvati M., Mannucci F., Stanga R. M., 1994, A&A, 292, 67
Jackson J. M., Eckart A., Cameron M., Wild W., Ho P. T. P., Pogge R. W., Harris A. I., 1991, ApJ, 375, 105
Jørgensen I., Franx M., Kjaergaard P., 1992, A&AS, 95, 489
Knapen J. H., 1996, in Proc. Nobel Symposium 98 *Barred Galaxies and Circumnuclear Activity*, Eds. Aa. Sandqvist, P.O. Lindblad, Lecture Notes in Physics, 474, 233, Springer-Verlag, Berlin
Knapen J. H., 1998, MNRAS, 297, 255
Knapen J. H., 1999, in Beckman J. E., Mahoney T. J., eds, The Evolution of Galaxies on Cosmological Timescales. Astron. Soc. Pac., San Francisco, Vol. 187, 72
Knapen J. H., Beckman J. E., Shlosman I., Peletier R. F., Heller C. H., de Jong R. S., 1995a, ApJL, 443, L73
Knapen J. H., Beckman J. E., Heller C. H., Shlosman I., de Jong R.S., 1995b, ApJ, 454, 623
Knapen J. H., Shlosman I., Heller C. H., Rand R. J., Beckman J. E. & Rozas, M., 2000, ApJ, 528, 219
Laine S., Knapen J. H., Pérez–Ramírez D., Shlosman I., Doyon R., Nadeau D., 1999, MNRAS, 302, L33.
McAlary C. W., McLaren R. A., Crabtree D. R., 1979, ApJ 234, 471
Maoz D., Barth A. J., Sternberg A., Filippenko A. V., Ho L. C., Macchetto F. D., Rix H.–W., Schneider D. P., 1996, AJ, 111 2248
Marcelin M., Boulesteix J., Georgelin Y., 1983, A&A, 128, 140
Martin P., Friedli D., 1997, A&A, 326, 449
Morgan, W.W., 1958, PASP, 70, 364
Nadeau D., Murphy D. C., Doyon R., Rowlands N., 1994, PASP, 106, 909
Peletier R. F., Knapen J. H., Shlosman I., Pérez–Ramírez D., Nadeau D., Doyon R., Rodriguez Espinosa J. M., Pérez García A. M., 1999, ApJS, 125, 363
Pérez, E., Márquez, I., Marrero, I., Durret, F., González Delgado, R.M., Masegosa, J., Maza, J., Moles, M., 2000, A&A 353, 893
Pérez–Ramírez D., Knapen, J.H., 2000a, MNRAS, submitted (Paper II)
Pérez–Ramírez D., Knapen, J.H., 2000b, MNRAS, in preparation (Paper III)
Phinney E. S., 1994, in Shlosman I., ed, Mass-Transfer Induced Activity in Galaxies. Cambridge: Cambridge Univ. Press, 1
Piner B. G., Stone J. M., Teuben P. J., 1995, ApJ, 449, 508
Pogge R. W., 1989a, ApJS, 71, 433
Pogge R. W., 1989b, ApJ, 345, 730
Pompea, S.M., Rieke, G.H., 1990, ApJ, 356, 416
Prendergast, K.H., 1962, in Distribution and Motion of ISM in Galaxies, ed. L. Wotljer (New York: Benjamin), 217
Quillen A. C., Alonso-Herrero A., Rieke M. J., McDonald C., Falcke H., Rieke, G.H. 1999, ApJ, 525, 685
Regan M. W., Elmegreen D. M., 1997, AJ, 114, 965
Regan M. W., Mulchaey J. S., 1999, AJ, 117, 2676
Reynaud D., Downes D., 1997, A&A, 319, 737
Reynaud D., Downes D., 1998, A&A, 337, 671
Reynaud D., Downes D., 1999, A&A, 347, 37
Ryder S. D., Knapen J. H., 1999, MNRAS, 302, L7
Sanders R. H., Teuben P. J., van Albada G. D., 1983, in Athanassoula E., ed, Proc. IAU Symp. 100, Internal kinematics and dynamics of galaxies. Reider, Dordrecht, p. 211
Sersic J. L., Pastoriza M. G., 1967, PASP, 79, 152
Shaw M. A., Axon D. J., Probst R., Gatley I., 1995, MNRAS, 274, 369
Shlosman I., 1999, in Beckman J. E., Mahoney T. J., eds, The Evolution of Galaxies on Cosmological Timescales. Astron. Soc. Pac., San Francisco, Vol. 187, 100
Shlosman I., Frank J., Begelman M. C., 1990, Nature, 345, 679
Simons D. A., Depoy D. L., Becklin E. E., Capps R. W., Hodapp K.–W., Hall D.N.B., 1988, ApJ, 335, 126
Spinoglio L., Malkan M. A., Rush B., Carrasco L., Recillas–Cruz E., 1995, ApJ, 453, 616
Taniguchi Y., 1999, ApJ, 524, 65
Taniguchi Y., Wada K., 1996, ApJ, 469, 581
Telesco C. M., Dressel L. L., Wolstencroft R. D., 1993, ApJ, 414,120
Wada K., Sakamoto K., Minezaki T., 1998, ApJ, 494, 236
Willner S. P., Elvis M., Fabbiano G., Lawrence A., Ward M. J., 1985, ApJ, 299, 443
Wozniak H., Friedli D., Martinet L., Martin P., Bratschi P., 1995, A&AS, 111, 115
Wynn–Williams C. G., Becklin E. E., 1985, ApJ, 290, 108

This paper has been produced using the Royal Astronomical Society/Blackwell Science LaTeX style file.

This figure "perezfig1.gif" is available in "gif" format from:

http://arxiv.org/ps/astro-ph/0004108v1